

Response of microchannel plates in ionization mode to single particles and electromagnetic showers

A. Yu. Barnyakov^{a,b,c}, M. Yu. Barnyakov^{a,b}, L. Brianza^d, F. Cavallari^e, M. Cipriani^{e,f}, V. Ciriolo^d, D. del Re^{e,f}, S. Gelli^{e,f}, A. Ghezzi^d, C. Gotti^d, P. Govoni^d, A. A. Katcin^{a,b}, M. Malberti^d, A. Martelli^{d,1}, B. Marzocchi^{e,f}, P. Meridiani^e, G. Organtini^{e,f}, R. Paramatti^{e,f}, S. Pigazzini^d, F. Preiato^{e,f}, V. G. Prisekin^{a,b}, S. Rahatlou^{e,f}, C. Rovelli^{e,*}, F. Santanastasio^{e,f}, T. Tabarelli de Fatis^d

^a*Budker Institute of Nuclear Physics, Lavrentieva 11, Novosibirsk 630090, Russia*

^b*Novosibirsk State University, Pirogova 2, Novosibirsk 630090, Russia*

^c*Novosibirsk State Technical University, Karla Marksa 20, Novosibirsk 630073, Russia*

^d*Università di Milano-Bicocca and INFN, Sezione di Milano-Bicocca, Piazza della Scienza 3, 20126, Milano, Italy*

^e*INFN, Sezione di Roma, Piazzale A. Moro 2, 00185, Roma, Italy*

^f*Sapienza, Università di Roma, Piazzale A. Moro 2, 00185, Roma, Italy*

Abstract

Hundreds of concurrent collisions per bunch crossing are expected at future hadron colliders. Precision timing calorimetry has been advocated as a way to mitigate the pileup effects and, thanks to their excellent time resolution, microchannel plates (MCPs) are good candidate detectors for this goal. We report on the response of MCPs, used as secondary emission detectors, to single relativistic particles and to electromagnetic showers. Several prototypes, with different geometries and characteristics, were exposed to particle beams at the INFN-LNF Beam Test Facility and at CERN. Their time resolution and efficiency are measured for single particles and as a function of the multiplicity of particles. Efficiencies between 50% and 90% to single relativistic particles are reached, and up to 100% in presence of a large number of particles. Time resolutions between 20 ps and 30 ps are obtained.

Keywords: Microchannel plates, secondary emission,

*Corresponding author: chiara.rovelli@roma1.infn.it

¹Now at CERN

1. Introduction

The projected beam intensity of future hadron colliders [1][2] will result in several hundreds of concurrent collisions per bunch crossing, spread over a luminous region of a few centimeters along the beam axis and of about a few 100 ps in time. The scientific program at these colliders, which includes precision characterization of the Higgs boson, measurements of vector boson scattering, and searches for new heavy or exotic particles, will benefit greatly from the enormous dataset. However, particle reconstruction and correct assignment to primary interaction vertices at high vertex densities presents a formidable challenge to the detectors that must be overcome in order to harvest that benefit. Time tagging of minimum ionizing particles (MIPs) and of neutral particles in the calorimeters with a resolution of a few 10 ps provides further discrimination of the interaction vertices in the same bunch crossing, beyond spatial tracking algorithms [3].

Among other sensors that are being investigated for precision timing of charged tracks, microchannel plates (MCPs) [4], renowned for their fast response, have been advocated as a candidate detector to time tag electromagnetic showers and MIPs and tested with moderate success [5][6][7][8]. In a previous work [9], we reported time resolutions of about 50 ps with cosmic muons and efficiencies of about 50% in the detection of single relativistic charged particles. The detectors consisted in a stack of two MCP layers with the dual function of seeding the cascade process, via the secondary electrons extracted from the MCP surface by the incoming ionizing particle, and of providing signal amplification. Similar studies [10][11][12] reported results comparable to ours for MIPs and virtually full efficiency in the detection of electromagnetic showers, at shower depths where the track multiplicity is high, with time resolutions at the level of a few tens of ps. In this paper, we further characterize the re-

sponse of MCPs in the direct detection of ionizing particles, hereafter referred to as ‘ionization-MCPs’ or shortly ‘i-MCPs’. The potential advantage of i-MCPs consists in the elimination of the photocathode, resulting in a easier and more robust construction and in a potentially larger radiation tolerance. We report on the dependence of the i-MCP performance on the stack geometry (number of layers or aspect ratio) and the use of MCP with high emissivity layers is also investigated. Several different prototypes of i-MCP detectors were exposed to charged particles beams. After the description of the detectors and of the measurement setup (Sec. 2 and Sec. 3) we present results in terms of efficiency and time resolution in response to single particles (Sec. 4). We report also about the behaviour of i-MCP prototypes in response to electromagnetic showers at different depths (Sec. 5). Due to their excellent time response, indeed, a layer of MCPs embedded in a calorimeter or in a preshower could be exploited to provide a precise time response for photons.

2. Detectors description and operation

The usage of MCPs as secondary electron emitters is investigated using either sealed MCP devices developed at BINP (Novosibirsk) in collaboration with the Ekran FEP manufacturer [13] or layers by the Photonis and Incom manufacturers mounted inside a vacuum chamber (with pressure kept below 10^{-5} mbar using a turbo molecular pump). The detectors are operated in ‘i-MCP mode’, therefore when a photocathode is present a retarding bias is applied to the gap between the photocathode itself and the MCP, as opposed to the standard ‘PMT-MCP’ mode. This prevents photoelectrons emitted from the photocathode from reaching the MCP surface and triggering an avalanche. In this configuration, the response of the detector is uniquely determined by the secondary emission of electrons from the MCP layers which are crossed by ionizing particles.

Devices are built with two, three or four layers of lead glass MCPs, except for one prototype made of borosilicate glass coated with emissive and resistive

layers. The channel diameter varies in the range from $3.5 \mu\text{m}$ to $25 \mu\text{m}$, and its ratio to the layer thickness (aspect ratio) ranges from 1:40 to 1:90 depending on the prototype. The channels have a bias angle to the photodetector axis of a few degrees. Two different electrical configurations are tested, which are sketched in Fig. 1.

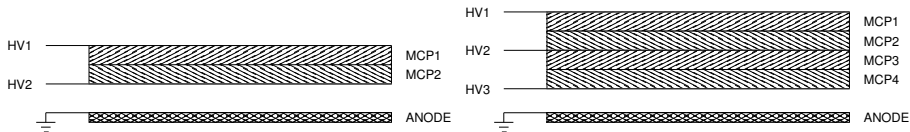


Figure 1: Sketch of the two electrical configurations under test: without separation of the emission and amplification stages (left) and with separated stages (right).

In the first one, same as in [9], a voltage divider is used to provide about 90% of the voltage drop through the entire MCP stack (2 or 3 layers). The layers carry out the dual function of seeding the cascade process, via secondary electrons extracted from the MCP, and providing signal amplification. In the second configuration the MCP layers are separated by the presence of electrodes, dividing a stage where the emission happens with large probability from the amplification stage. More details on this approach will be given in the following.

The specifications of the detectors are detailed in Tab. 1 and Tab. 2 for the two configurations. The prototypes which are mounted inside a vacuum chamber (VC) have slightly less than one radiation length of material in front due to the steel flange closing the chamber.

3. Experimental setup

The i-MCP detectors were exposed to particle beams, in order to characterize their response to single particles and electromagnetic showers in terms of detection efficiency and time resolution.

The devices without separation of the emission and amplification stages were tested at the H4 [14] and H2 [15] beam lines at the CERN North Area. The electron beam at the H4 Area is extracted from the CERN SPS and can be

| Device | Assembly | Layers | Diameter | Aspect ratio |
|--------------|----------|--------|-------------------|--------------|
| 40×2 | Sealed | 2 | 12 μm | 1:40 |
| 40×3 | Sealed | 3 | 8 μm | 1:40 |
| <i>SEE</i> | Sealed | 2 | 7.5 μm | 1:40 |
| <i>MGO</i> | VC | 2 | 10 μm | 1:40 |

Table 1: Devices without separation of the emission and amplification stages. The designation given to each device indicates either the aspect ratio times the number of layers or the superficial treatment applied (secondary emission enhancement *SEE* or atomic layer deposition with Magnesium oxide *MGO*).

| Device | Assembly | Layers | Em.Layer 1 | Em.Layer 2 | Ampl.Layer 1 | Ampl.Layer 2 |
|-------------------------|----------|--------|--------------------------|--------------------------|-------------------------|------------------------|
| $40\times 2+40\times 2$ | Sealed | 4 | 7 μm , 1:40 | 7 μm , 1:40 | 7 μm , 1:40 | 7 μm , 1:40 |
| $90\times 1+40\times 2$ | Sealed | 3 | 3.5 μm , 1:90 | - | 7 μm , 1:40 | 7 μm , 1:40 |
| $90\times 2+40\times 2$ | Sealed | 4 | 3.5 μm , 1:90 | 3.5 μm , 1:90 | 7 μm , 1:40 | 7 μm , 1:40 |
| $80\times 2+40\times 1$ | VC | 3 | 25 μm , 1:80 | 25 μm , 1:80 | 25 μm , 1:40 | - |
| $80\times 1+40\times 1$ | VC | 2 | 8 μm , 1:80 | - | 10 μm , 1:40 | - |

Table 2: Devices operated with separated emission and amplification stages. For each layer the channel diameter and the aspect ratio are quoted. The designation given to each device indicates the aspect ratio times the number of layers for the emission stage (first part) and for the amplification stage (second part).

tuned in the momentum range from 10 GeV to 200 GeV. Our efficiency and time resolution measurements were performed with 20 GeV and 50 GeV electrons. The MCP devices were mounted in a box with the optical window orthogonal to the beam direction. Signals were read from a 32-channels digitizer (CAEN V1742) with 5 GHz sampling frequency. A hodoscope was placed along the beam line upstream of the MCPs and readout into a gated-ADC, for beam centering and offline selection purposes. It consisted of four planes with 64 parallel scintillating fibers each, 1 mm in diameter and staggered, covering an acceptance of $20\times 20\text{ mm}^2$ in the coordinates transverse to the beam. One of the MCPs along the beam line was operated in PMT-MCP mode, to provide a

trigger and a reference for the efficiency and time measurements. The H2 beam is a secondary particle beam extracted from the CERN SPS providing hadrons, electrons or muons of energies between 10 GeV and 360 GeV. In this case, our efficiency measurements were performed with 150 GeV muons with a similar setup as in H4.

The devices with separated emission and amplification stages were tested at the T9 area at CERN [16] and at the Beam Test Facility (BTF) of the INFN Laboratori Nazionali di Frascati (Italy) [17]. In the T9 Area a secondary beam with momentum range from 1 GeV to 5 GeV is originated from the CERN PS beam impacting on a target. Our measurements were performed on a beam of 2 GeV electrons (20%) and pions (80%). The experimental setup was similar to the one used at the North Area and a Cherenkov detector was used to separate the electron and pion components of the beam. The BTF in Frascati provides 10 ns long electron pulses with tunable energy (up to about 500 MeV), repetition rate (up to 49 Hz) and intensity (from 1 to 10^{10} particles per pulse). Our measurements were performed with 491 MeV electrons and an intensity tuned to provide an average of about one electron per pulse. A similar beam line equipment as in H4 was used, with only minimal differences. One MCP operated in PMT-MCP mode was placed upstream of the i-MCPs along the beam line and another one downstream, to select events going through the i-MCPs without showering. Also, a 5 mm thick plastic scintillator counter with an area of 24×24 mm² was installed in front of the MCPs, together with a hodoscope, to allow selecting events with single electrons impinging on the detectors. A schematic view of the BTF setup is shown in Fig. 2.

The MCP devices produce very fast signals, with a rise-time of the order of 1 ns. A typical MCP waveform is shown in Fig. 3, where the secondary peaks are due to an imperfect matching between the anode and the transmission line to the digitizer. For each event, a coincidence window of 60 ns is opened around the time corresponding to the maximum amplitude of the MCP operated in PMT-MCP mode acting as a trigger. The maximum of the waveform of the i-MCP under test is searched inside this window. The signal time information is

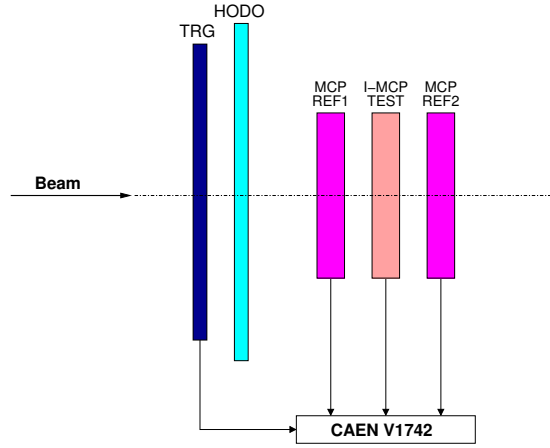


Figure 2: Schematic view of the MCPs and other equipments position along the beam line at the BTF in Frascati. A plastic scintillator counter (TRG) and a hodoscope (HODO) are put in front of the MCPs along the beam line. The i-MCP under study (i-MCP TEST) is put between two MCPs operated in PMT-MCP mode used as references (MCP REF1, MCP REF2).

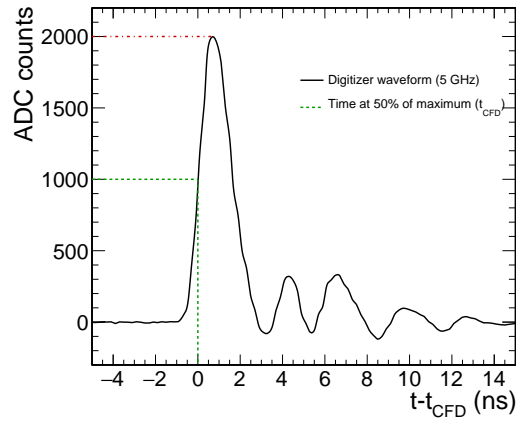


Figure 3: A typical MCP waveform as extracted from the digitizer (solid line). On the x-axis the time t_{CFD} for which the signal amplitude is 50% (dashed line) of its maximum value (dashed-dotted line) is subtracted as an offset.

extracted from the interpolated waveforms via a constant fraction discriminator (CFD), corresponding to the time when the amplitude is half of its maximum.

4. Response to single charged particles

To characterize the i-MCP detectors behaviour their efficiency and time resolution were first measured in response to single electrons and muons. Events consistent with a single particle are selected in the offline analysis requiring a pulse larger than 200 ADC counts in the reference PMT-MCP device. The hodoscope information is also used when available. At the BTF, the bunched beam structure requires a further selection for single electron events, identified from the pulse-height of the signal in the scintillator counter which is asked to be between 200 and 700 ADC counts. Furthermore, a signal between 200 and 1200 ADC counts is required in the PMT-MCP downstream of the i-MCP (the upper limit is set to discard events in which the electron makes a shower along the beam line). Typical spectra of the scintillator counter and of the PMT-MCP

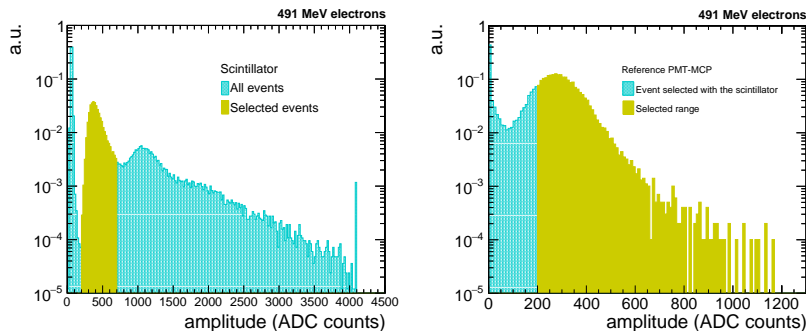


Figure 4: Typical ADC spectrum of the scintillator counter (left) and of the MCP operated in PMT-MCP mode and put as a first detector along the beam line (right) at the BTF. In the right plot, only the events selected based on the scintillator response are shown. The region corresponding to single electron events is shown as a filled histogram in both plots.

upstream of the test i-MCP at the BTF are shown in Fig. 4.

4.1. Efficiency of single-stage MCP stacks

The efficiency of each MCP is defined as the fraction of events with a signal above threshold with respect to the total number of single electron events, selected as discussed in the previous section. The threshold is defined as 5 times the noise of the detector, which is measured in pedestal runs or in events without electrons impacting on the scintillator. The efficiency of some prototypes exposed to the H4 beam and operated in i-MCP mode is shown in Fig. 5 on the left as a function of the MCP-stack bias. For a comparison, the efficiency of one of them operated in PMT-MCP mode is also shown.

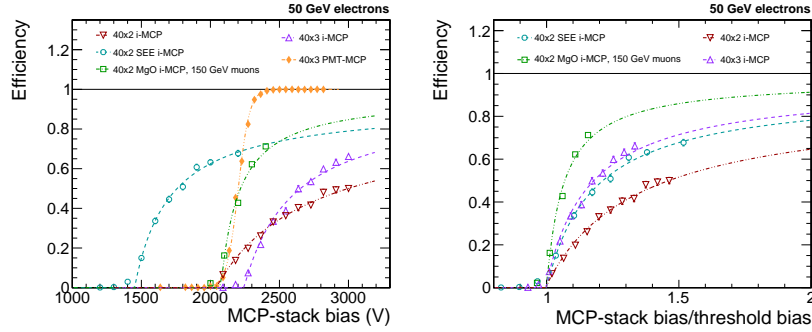


Figure 5: Left) Efficiency to 50 GeV electrons and 150 GeV muons of MCP detectors with direct (full dots) and retarding bias (empty dots, squares and triangles) between the photocathode and the first MCP layer as a function of the stack bias. For the detectors operated in i-MCP mode the curve through the points is a fit to data of the response model detailed in the text (Eq. 1). For the detector operated in PMT-MCP mode data are fitted with a Fermi-Dirac function. Right) Same efficiency as a function of the stack bias normalized to the threshold voltage, extracted from Eq. 1.

In PMT-MCP mode the photoelectrons are extracted from the photocathode and amplified above the detection threshold by the MCP. As it was found in [9], a 100% efficiency is obtained at plateau, where the MCP gain is high enough to supply single photoelectron detection. In i-MCP mode, the MCP layers have the dual function of initiating the cascade process and providing signal amplification. Different channel lengths are involved in the amplification process, depending on where the secondary electron is emitted, and inefficiencies

may arise either because of lack of secondary emission or because of insufficient amplification in the cascade following the secondary emission. A model was developed in our earlier work [9] in which the detection efficiency is parameterized as

$$\varepsilon = s \left(1 - \frac{1}{b \cdot \ln(V/V_{th}) + 1} \right), \quad (V \geq V_{th}) \quad (1)$$

under the hypothesis that the gain has a power-law dependence on the bias voltage. The model parameters V_{th} , s and b are extracted from data. The parameter s represents the probability of secondary emission over the entire MCP length and it is found to be compatible with one for the detectors under study. The parameter b describes the gain and depends on the device. V_{th} is the threshold voltage at which secondary electrons generated at the surface of the MCP receive the exact gain needed for detection. The behaviour of the efficiency versus the bias voltage can be explained with a change in the volume of the sensitive region, that is the region where an electron receives enough amplification to be detected as a signal. At the threshold voltage, the whole MCP length is needed in order to amplify the signal over a detectable threshold and the signal is detected only if the secondary emission occurs at the surface of the MCP. The efficiency increases with the bias voltage, since signals overcome the detection threshold also if the secondary emission occurs inside the MCP layers. The curves in Fig. 5 are extrapolated to voltage values which can not be currently reached due to the MCP electric strength.

The prototype with two layers (40×2) reaches a maximum efficiency of about 50% for single electrons, confirming the results in [9]. Adding a third layer (40×3) the efficiency raises up to about 70%, since the number of channel interfaces crossed by the particle is increased. As suggested in [9], and demonstrated in Fig. 5, the detection efficiency increases with the number of layers. However, even with three layers the curve is not at plateau, suggesting that the efficiency gain is too slow.

The efficiency is larger, for the same channel length, in i-MCPs with en-

hanced secondary emission yield. The *SEE* and *MGO* prototypes, also shown in Fig. 5, are two-layers i-MCPs. The *SEE* prototype underwent a surface treatment in order to increase the channel walls secondary emission efficiency. The *MGO* prototype is made of layers produced from a borosilicate glass substrate with an atomic layer deposition technique (ALD by INCOM Ltd [18][19]) and a final layer of Magnesium oxide. The *SEE* device reaches an efficiency of about 50% at a stack bias of about 1750 V, while for regular i-MCPs with 2 layers the same efficiency is reached at about 3000 V. Also, the efficiency raises up to about 70%. The same efficiency is reached for the *MGO* prototype. Owing to an accident while improving the test setup, we could not study the response of the *MGO* prototype at biases larger than 2400 V. The analysis however shows that with MgO coatings efficiencies as high as 90% could be attained still at moderate high voltages.

For all the i-MCP prototypes, data are well described by the model of Eq. 1, suggesting that the efficiency trend with the voltage does not depend on the specific characteristics of the detector. The universality of the model for single stage i-MCPs is further demonstrated in the right panel of Fig. 5, where the efficiency is shown as a function of the stack bias normalized to the threshold voltage, extracted from a fit of the functional form of Eq. 1 to the data.

4.2. Efficiency of multi-stage MCP stacks

An alternative way to improve the i-MCP behaviour consists in separating the region where the signal is created from the amplification stage, providing a separate bias for the two layers. This configuration is motivated by the fact that a few photoelectrons entering two or three MCP layers give a clear signal above noise, as demonstrated operating the detectors in PMT-MCP mode.

In Fig. 6 we show the efficiency of the multi-stage prototypes as a function of the MCP-stack bias, which is varied to change the response of the devices. The amplification stage voltage is fixed. For the detectors in the vacuum chamber ($80\times 1+40\times 1$, $80\times 2+40\times 1$) the probability for a single electron to originate a shower before reaching the MCP is not negligible. A correction factor is therefore

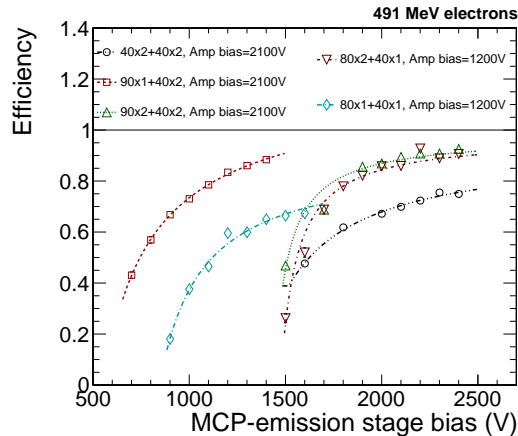


Figure 6: Efficiency to 491 MeV electrons of multi-stage MCP detectors operated in i-MCP mode. The efficiency is given as a function of the emission stage bias, while the amplification stage bias is reported in the legend. The curve through the points is a fit to data of the response model detailed in the text (Eq. 3).

computed using the data collected at the T9 beam area, where one of the i-MCPs was exposed to a mixed beam of electrons and pions. The electron and pion components were separated with a Cherenkov detector and the efficiency in response to each component was computed. The i-MCP efficiency in response to electrons is larger than to pions, which means that also electrons produced in the primary electron cascade may generate a signal. Describing the i-MCP response with a binomial per-event probability

$$\varepsilon_n = 1 - (1 - \varepsilon_1)^n, \quad (2)$$

where ε_1 is the efficiency to single particles and n is the multiplicity of electrons per electron crossing the MCP, we find an average n of about 1.4. The efficiencies measured at the BTF on the i-MCPs inside vacuum chambers are corrected for this factor, neglecting the difference in moving from 2 GeV to 491 MeV.

Three of the multi-stage MCPs have the same amplification region, consisting of two layers with aspect ratio 40:1 (40×2) operated at a voltage around 2100 V. The efficiency of these MCPs in response to charged particles does not

reach zero even at low stack bias, the residual efficiency being given by the amplification stage itself. Experimental results suggest that the efficiency is larger using layers with large aspect ratio in the emission stage ($90\times 2+40\times 2$, $90\times 1+40\times 2$). An efficiency larger than 90% is reached in the configuration $90\times 2+40\times 2$, which is almost 20% larger than with small aspect ratio, e.g. $40\times 2+40\times 2$. In the other two chambers the amplification region consists of one layer with aspect ratio 40:1 (40×1). Also in this case, the efficiency increases by 20% adding an extra layer in the emission stage ($80\times 2+40\times 1$ with respect to $80\times 1+40\times 1$). In summary, the efficiency can be increased either building chambers with thicker layers or adding extra layers. Since the prototypes 40×3 , discussed in Section 4.1, and $80\times 1+40\times 1$ reach similar efficiencies, the relevant factor appears to be only the total thickness, independently of the number of layers which are employed. Finally, the prototypes $90\times 2+40\times 2$ and $80\times 2+40\times 1$ reach the same plateau efficiency, while the efficiency at low bias voltage is larger for the stack with an additional amplification layer. This suggests that the addition of extra layers in the amplification stage gives only a small contribution to the total efficiency if the efficiency of the emission stage is large enough.

The efficiency as a function of the emission stage bias (HV) for multi-stage i-MCPs is parameterized in Fig. 6 as

$$\varepsilon = P_{amp}(1 - P_{em}(HV)) + P_{em}(HV) \quad (3)$$

P_{amp} is the contribution of the amplification layer only, which may have an efficiency larger than zero even when no electron is generated in the emission layers and which does not depend on the voltage of the emission stage. P_{amp} is compatible with zero for the devices where the amplification stage is made of a single layer MCP, and it is slightly above 20% for the devices with double layer amplification stage. P_{em} may be parameterized as in Eq. 1. This model well describes the data as a function of the voltage of the emission stage, which suggests that the parameterization in Eq. 1 works well for every single stage i-MCP detector.

4.3. Time resolution

The time resolution of i-MCP detectors exposed to a single particle beam is extracted comparing the time of the detector under study with the time of a reference MCP operated in PMT-MCP mode and put upstream of the i-MCPs along the beam line. Pulses consistent with a single electron entering the test setup are selected in the same way as for the efficiency measurement. The signal time information is estimated with the CFD method and only the events where the time of the i-MCP detector is compatible with the time of the reference PMT-MCP within 1 ns are retained for the analysis.

When a detector is operated in i-MCP mode, differently from the PMT-MCP mode case, time non-linearities as a function of the signal amplitude arise. The time difference between signals with low and large amplitude is compatible with a fraction of the transit time, which is around 200-300 ps, therefore it is reasonable to assume that the signals with low amplitude are in average created closer to the anode than larger signals. This effect, which is shown in Fig. 7 on the left, is corrected for with an empirical function. The distribution of the time

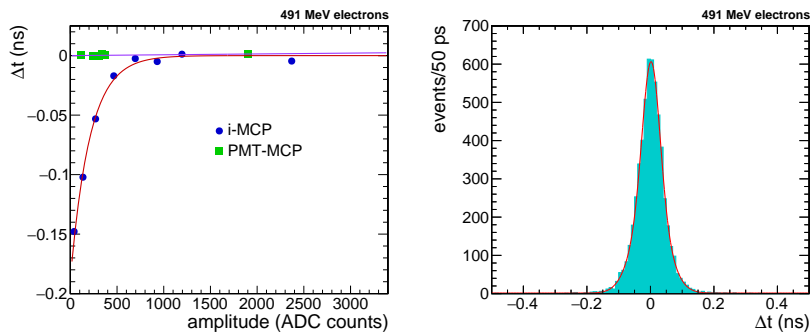


Figure 7: Left: Difference between the time of a MCP detector, operated either in i-MCP mode (dots) or PMT-MCP mode (squares), and the time of a reference detector operated in PMT-MCP mode as a function of the signal amplitude. Right: Distribution of the time difference between the signals measured in two MCPs, one operated in i-MCP mode and the other one in PMT-MCP mode. Both plots refer to MCPs exposed to 491 MeV electrons.

difference between the $90 \times 1 + 40 \times 2$ detector operated in i-MCP mode and the

reference PMT-MCP, after the non-linearity correction, is shown in Fig. 7 on the right in response to 491 MeV electrons and for an operating voltage of 1400 V. To compute the i-MCP time resolution a Gaussian fit to this distribution is performed, then the resolution of the reference PMT-MCP is subtracted. The latter is extracted comparing the relative resolution of the time difference with respect to another PMT-MCP detector and with respect to an i-MCP detector. It is found to be 17 ± 2 ps.

Fig. 8 shows the time resolution of the $90\times 1+40\times 2$ i-MCP detector as a function of the signal over noise ratio, after the resolution of the reference PMT-MCP is subtracted. The trend can be parametrized as

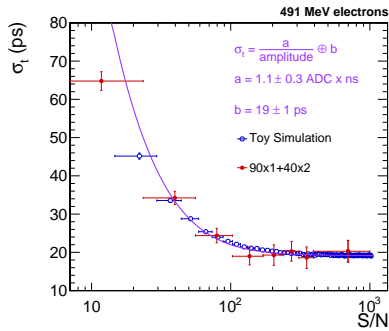


Figure 8: Time resolution for an i-MCP prototype exposed to 491 MeV electrons as a function of the signal over noise ratio. The resolution of the reference MCP operated in PMT-MCP mode is subtracted.

$$\sigma = \frac{a}{S/N} \oplus b, \quad (4)$$

from which the noise component a and the constant term b of the resolution are extracted. The parameter b determines the best resolution which can be achieved and it mainly depends on the transit time spread, i.e. the time difference due to the different paths followed by the electrons in reaching the anode. Other sources can also contribute, like imperfections in the time reconstruction or in the non-linearity corrections. In Fig. 8 data are compared to a toy simulation which is based on a pulse shape template built from data. Uncorrelated

noise is added to each sample as extracted from a pedestal run. The noise contribution a measured in data is compatible with the expectations from simulation. The current simulation does not contain sources which can contribute to the constant term, so a Gaussian smearing is added to match the data. The time resolution averaged over all the signal amplitudes is 26 ± 2 ps for this device. For a comparison, the time resolution for single photoelectron events of the same device operated in PMT-MCP mode and measured with a laser is 24 ps [20].

The average time resolution and the constant term of Eq. 4 were computed for all the devices under test. The results are compatible among the different prototypes and constant terms between 20 ps and 30 ps are obtained in all cases. Only a small dependence of the time resolution on the number of layers and their aspect ratio is observed. The data collected do not allow a systematic study of the time resolution dependence on the channel diameter and layer thickness.

5. Response to electromagnetic showers

To characterize the i-MCP response to electromagnetic showers, data were acquired with a set of absorbers of variable thickness and up to almost 5 radiation lengths X_0 in front of the detector. The tests were performed at the CERN H4 Area.

The evolution of the efficiency to detect 20 GeV electrons is shown in Fig. 9 on the left for a 3 layers i-MCP as a function of the absorber thickness in units of X_0 . The efficiency definition is the same as in Sec. 4. The device was operated at the maximum voltage used in the bias voltage scan performed in the single particle setup, corresponding to the highest detection efficiency in that configuration. The efficiency increases with the thickness of the absorber, reaching 95% after $1X_0$ and close to 100% after $2X_0$. These results, which confirm the indications in [9], are promising in view of the usage of the i-MCP detectors in calorimeters at hadron colliders.

The time resolution in response to electromagnetic showers initiated by

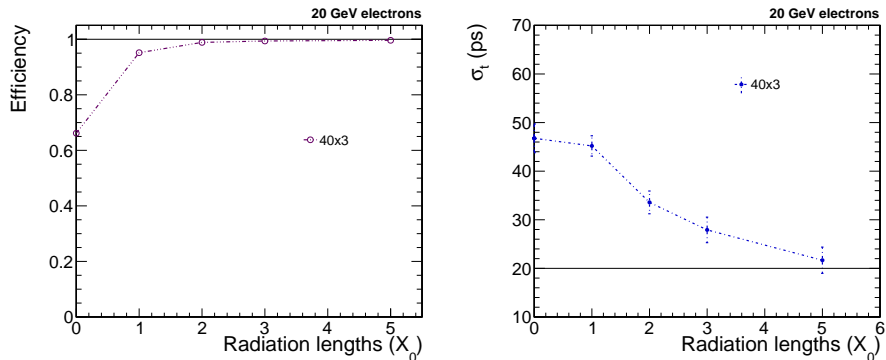


Figure 9: Efficiency (left) and time resolution (right) of MCP prototypes operated in i-MCP mode and exposed to 20 GeV electrons as a function of the absorber thickness, in units of radiation lengths. The contribution of the reference MCP to the time resolution is subtracted.

20 GeV electrons is shown as a function of the shower depth in Fig. 9 on the right, after the removal of the contribution of the reference MCP resolution. Due to the increased multiplicity of charged particles the digitizer input can saturate and in this case the time to cross a fixed threshold of 500 ADC counts is used as time estimate, instead of the CFD algorithm. The same event selection as in Sec. 4.3 is used. Fig. 9 refers to a different detector with respect to the one used as an example in the previous section, with a larger noise but comparable constant term. This explains why the time resolution at $0X_0$ is worse than in Fig. 8 when averaging over all the signal amplitudes. The time resolution improves as expected with the absorber thickness, because the MCP layers are crossed by a larger multiplicity of particles. An inclusive time resolution of about 20 ps is reached after $5X_0$.

6. Summary and outlook

We report on the response of microchannel plates to single relativistic particles and to electromagnetic showers. Several prototypes of MCPs used as secondary emission detectors were exposed to particle beams at the INFN-LNF Beam-Test Facility and at CERN. Configurations with multiple MCP stacks,

different geometries or layer coatings were compared, to investigate how these aspects affect the total amount of secondary emission and the channel gain. In the tested configurations, detection efficiencies to single relativistic particles between 50% and 90% and constant terms for the time resolution between 20 ps and 30 ps are reached. Measurements with electromagnetic showers sampled at different depths show that, in presence of a large enough number of particles, detection efficiencies up to 100% can be reached with average time resolutions as good as 20 ps, independently of the geometry. Present results suggest that this detection technique is suitable for a precise determination of the time of high energy photons and charged particles, and could help in the event reconstruction at high luminosity colliders.

7. Acknowledgements

We warmly thank R. Bertoni, R. Mazza, M. Nuccetelli and F. Pellegrino for the preparation of the experimental setup. We are indebted to B. Buonomo, C. Di Giulio, L. Foggetta and P. Valente for their help with the setup of the beam facility at Frascati. We are grateful to the CERN PS and SPS accelerator teams for providing excellent beam quality. This research program is carried out in the iMCP *R&D* project, funded by the Istituto Nazionale di Fisica Nucleare (INFN) in the Commissione Scientifica Nazionale 5 (CSN5). It has also received funding from the European Union Horizon 2020 research and innovation programme under the Marie Skłodowska-Curie grant agreement No 707080. The production of tested BINP design exemplars and carrying out their measurements in Novosibirsk was supported by the Russian Science Foundation (Project no.16-12-10221).

References

References

- [1] G. Apollinari et al., High-Luminosity Large Hadron Collider (HL-LHC): Preliminary Design Report, CERN Yellow Reports: Monographs, 2015

- [2] M. Benedikt, F. Zimmermann, Future Circular Colliders, CERN-ACC-2015-164, 2015
- [3] B. Bezverkhny Abelev et al., Performance of the ALICE Experiment at the CERN LHC., *Int.J.Mod.Phys.*, A29:1430044, 2014, doi:10.1142/S0217751X14300440
- [4] J. L. Wiza, Microchannel plate detectors, *Nucl.Instrum.Meth.*, 162:587, 1979
- [5] A. A. Derevshchikov et al., On possibility to make a new type of calorimeter: Radiation resistant and fast, *Report, IFVE-90-99, Protvino*, 1990
- [6] M. Bondila et al., Results of in-beam tests of an MCP-based vacuum sector prototype of the T0/centrality detector for ALICE, *Nucl.Instrum.Meth.* A478:220-224, 2002, doi:10.1016/S0168-9002(01)01761-2
- [7] B. Adams et al., Measurements of the gain, time resolution, and spatial resolution of a 20x20cm² MCP-based picosecond photo-detector, *Nucl.Instrum.Meth.* A732:392-396, 2013, doi:10.1016/j.nima.2013.07.091
- [8] B. Adams et al., A Brief Technical History of the Large-Area Picosecond Photodetector (LAPPD) Collaboration, arXiv:1603.01843
- [9] L. Brianza et al., Response of microchannel plates to single particles and to electromagnetic showers, *Nucl.Instrum.Meth.* A797:216-221, 2015, doi:10.1016/j.nima.2015.06.057
- [10] R. Ronzhin et al., Development of a new fast shower maximum detector based on microchannel plates photomultipliers (MCP-PMT) as an active element, *Nucl.Instrum.Meth.* A759:65-73, 2014, doi:10.1016/j.nima.2014.05.039
- [11] R. Ronzhin et al., Direct tests of micro channel plates as the active element of a new shower maximum detector, *Nucl.Instrum.Meth.* A795:52-57, 2015, doi:10.1016/j.nima.2015.05.029

- [12] A. Apresyan et al., Direct tests of a pixelated microchannel plate as the active element of a shower maximum detector, *Nucl. Instrum. Meth.* A828:1-7, 2016, doi:10.1016/j.nima.2016.05.015
- [13] A. Yu. Barnyakov et al., Investigation and development of microchannel plate phototubes, *Nucl.Instrum.Meth.* A572:404-407, 2007, doi:10.1016/j.nima.2006.10.276
- [14] <http://sba.web.cern.ch/sba/BeamsAndAreas/resultbeam.asp?beamline=H4>
- [15] <http://sba.web.cern.ch/sba/BeamsAndAreas/h2/H2manual.html>
- [16] L.Durieu, M.Martini and A.-S.Muller, Optics studies for the T9 beam line in the CERN PS East Area secondary beam facility, Proceedings of the 2001 Particle Accelerator Conference, Chicago
- [17] A. Ghigo et al., Commissioning of the DAFNE beam test facility. *Nucl.Instrum.Meth.* A515:524-542, 2003
- [18] S. J. Jokela et al., Secondary Electron Yield of Emissive Materials for Large-Area Micro-Channel Plate Detectors: Surface Composition and Film Thickness Dependencies, *Physics Procedia*, 37:740-747, 2012, doi:10.1016/j.phpro.2012.03.718
- [19] A. U. Mane et al., An Atomic Layer Deposition Method to Fabricate Economical and Robust Large Area Microchannel Plates for Photodetectors, *Physics Procedia*, 37:722-732, 2012, doi:10.1016/j.phpro.2012.03.720
- [20] A. Yu. Barnyakov et al., Micro-channel plates in ionization mode as a fast timing device for future hadron colliders, to be published in JINST, Int. Conf. Instrumentation for Colliding Beam Physics, 28 Feb. - 3 Mar., 2017, Novosibirsk, Russia.